*Supporting Information*

Modulating the Electronic Properties of Monolayer Graphene Using a Periodic Quasi-One-Dimensional Potential Generated by Hex-Reconstructed Au(001)

Xiebo Zhou[1,2], Yue Qi[2], Jianping Shi[1,2], Jingjing Niu[3], Mengxi Liu[2], Guanhua Zhang[4] Qiucheng Li[2], Zhepeng Zhang[2], Min Hong[1,2], Qingqing Ji[2], Yu Zhang[1,2], Zhongfan Liu[2], Xiaosong Wu[3*], Yanfeng Zhang[1,2*]

[1.] Department of Materials Science and Engineering, College of Engineering, Peking University, Beijing 100871, People's Republic of China

[2.] Center for Nanochemistry (CNC), Beijing National Laboratory for Molecular Sciences, College of Chemistry and Molecular Engineering, Academy for Advanced Interdisciplinary Studies, Peking University, Beijing 100871, People's Republic of China

[3.] State Key Laboratory for Artificial Microstructure and Mesoscopic Physics, Peking University, Beijing 100871, P. R. China, Collaborative Innovation Center of Quantum Matter, Beijing 100871, People's Republic of China

[4.] State Key Laboratory of Molecular Reaction Dynamics, Dalian Institute of Chemical Physics, Chinese Academy of Sciences, Dalian 116023, People's Republic of China

[*] Address correspondence to Yanfeng Zhang (yanfengzhang@pku.edu.cn), Xiaosong Wu (xswu@pku.edu.cn)
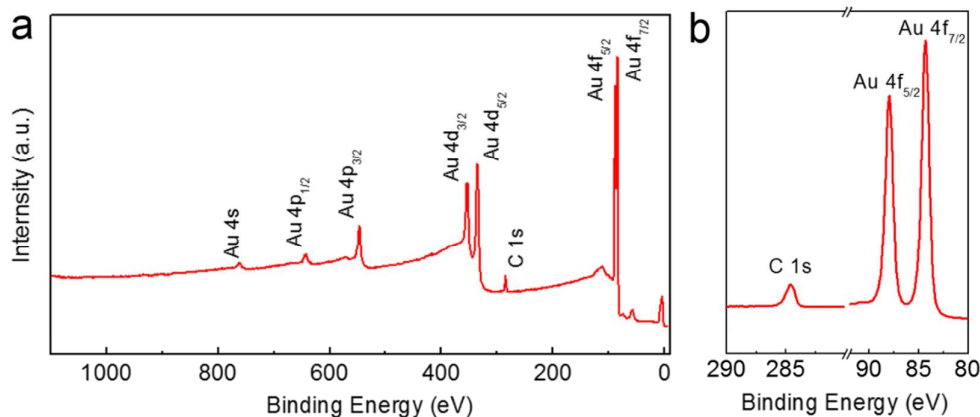
Figure S1. XPS spectra of the as-grown graphene/Au foil sample. (a) XPS spectra over a wide range of the binding energy (0 – 1,000 eV). (b) Detailed XPS spectra obtained from the binding energy from 80 eV to 290 eV.

We can find that well defined XPS peaks occur at 84.5 eV and 87.9 eV, corresponding to the $4f_{7/2}$ and $4f_{5/2}$ peaks of Au.[1] And the evidence for the formation of graphene can be defined from the presence of C 1s peak at 284.6 eV, as shown in **Figure S1b**. This data is in good agreement with the previous reference.[2]
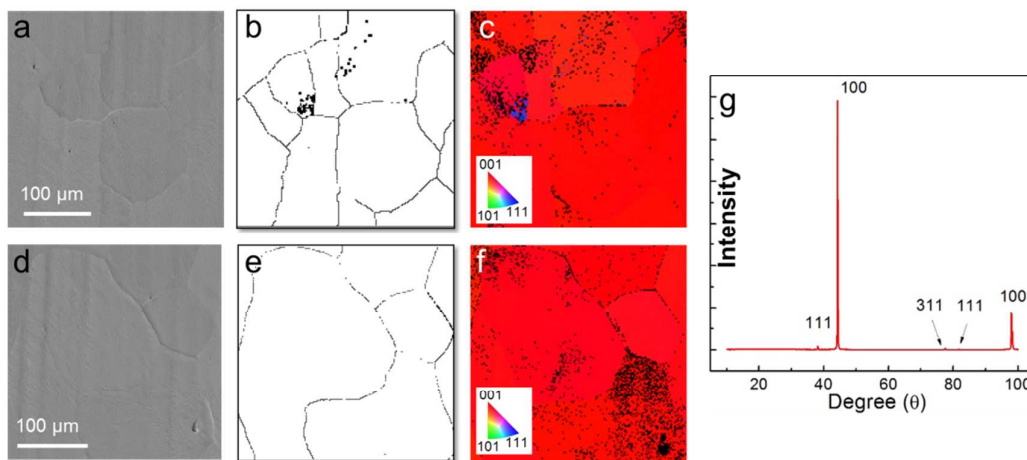
Figure S2 Facet compositions of the Au foils after graphene growth. (a, b) SEM image and the grain boundary distribution (defined from the corresponding SEM image in (a) of graphene/Au foils. (c) Corresponding Electron Backscattered Diffraction (EBSD) orientation map of the same area in (a). (d, e) SEM image and the corresponding grain boundary distribution of a different location of the sample. (f) Corresponding EBSD orientation map of the location in (d). (g) X-ray diffraction

(XRD) data from the same sample.

Here, we show SEM and EBSD maps of two locations of the graphene/Au foil sample, which has been annealed by two processes. Firstly, the graphene/Au foil sample has been annealing in the CVD tube at ~0.1 Pa for 10 hours which resembling the pre-annealing process of Au foils before graphene growth. Secondly, a ~800°C annealing progress in ultrahigh vacuum (UHV) (~1.0E-11 torr) chamber has been executed for 4 hours, which resembles the post-annealing process for the samples used for STM characterizations.

Typical SEM images and EBSD maps of the graphene/Au foils are presented in the new **Figure S2**, with **Figure S2a-c** and **Figure S2d-f** captured from the different locations of the sample. From the SEM images shown in **Figure S2a, d**, the grain boundaries of the Au foils can be visualized very clearly, and the grain size is sometimes larger than 100 μm × 100 μm. Interestingly, although almost 13 grains exist in **Figure S2a-c** and 7 grains in **Figure S2d-f**, they are all (001) facets as revealed by the EBSD color bar. Moreover, the XRD data of the same sample also justifies the existence of the (001) facet. Notably, some other facets like (111) and (311) facets contribute only a minor portion of the surface, as shown in **Figure S2g**.

Additionally, as presented in **Figure S2(c)**, there is a blue area in the central region, which should be attributed to the Au(111) facet. And the black-spot regions in the EBSD orientation map are those regions which could not be resolved definitely by the equipment (Merlin).

The reason for the formation of Au(001) facets after graphene growth is much complex. There are many factors which may influence the metal foil's texture. The surface energy is believed to be one of the most important factor, the lower surface energy of the facet domain, the larger it grows.[3,4] Moreover, the surface energy can be variable with the sample annealing conditions. For instance, under certain annealing atmosphere (*e.g.* the presence of oxygen) a grain with a (110) plane appears to have lower surface energy than that with (100). And under another atmosphere (for example, vacuum), this relationship can be reversed so that (100) grains are more

favored.[5,6]

In this regard, we believe that the hex-reconstructed Au(001) has the lowest surface energy in our annealing condition under the vacuum, thus the surface tends to be mainly composed by (001) textures.
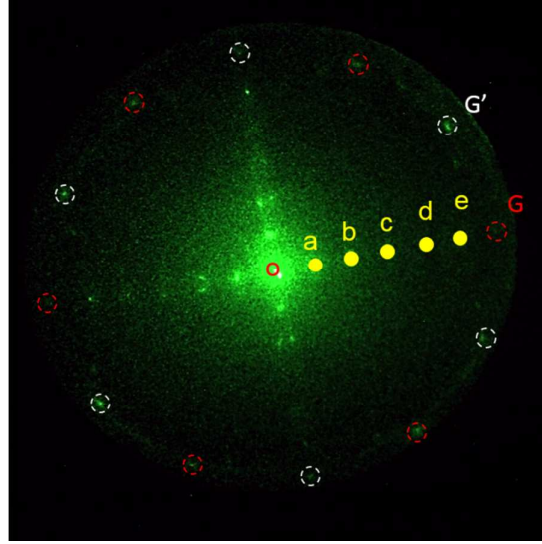

Figure S3 *Low energy electron diffraction (LEED) pattern of the graphene on reconstructed Au(001).*

The LEED pattern is also taken from the UHV-annealed samples, i.e., through ~800°C annealing for about 4 hours. The outer hexagonally arranged spots marked as red and white should originate from two graphene domains rotated by 30° with each other (labeled as G and G'), as similarly observed by the selected area electron diffraction (SAED) patterns in supporting information **Figure S4.** The inner spots are tetragonal, and the outer spots can be marked in one direction with yellow circles (labeled as letters from "a" to "e", the central point is "o"). We measure the ratio of $|\mathbf{oe}| / |\mathbf{oG}| = 1.19$, which matches well with the ratio of $\mathbf{a}_{Au(001)} / \mathbf{a}_{graphene} = 0.288\text{nm} / 0.246\text{nm} = 1.17$. This result convinces the existence of the Au(001) facet.

Moreover, for the a, b, c and d diffraction spots, they equally divide $|\mathbf{oe}|$ into five parts, which means the existence of a striped reconstruction having a periodicity about $5 \times 0.288 = 1.44$ nm, in line with distance of the striped modulation. With this diffraction data, the hex-reconstruction of Au(001) is proposed to be positioned below

4

the graphene layer. Notably, this LEED pattern has already been reported for the pure hex-reconstruction of Au(001).[7]
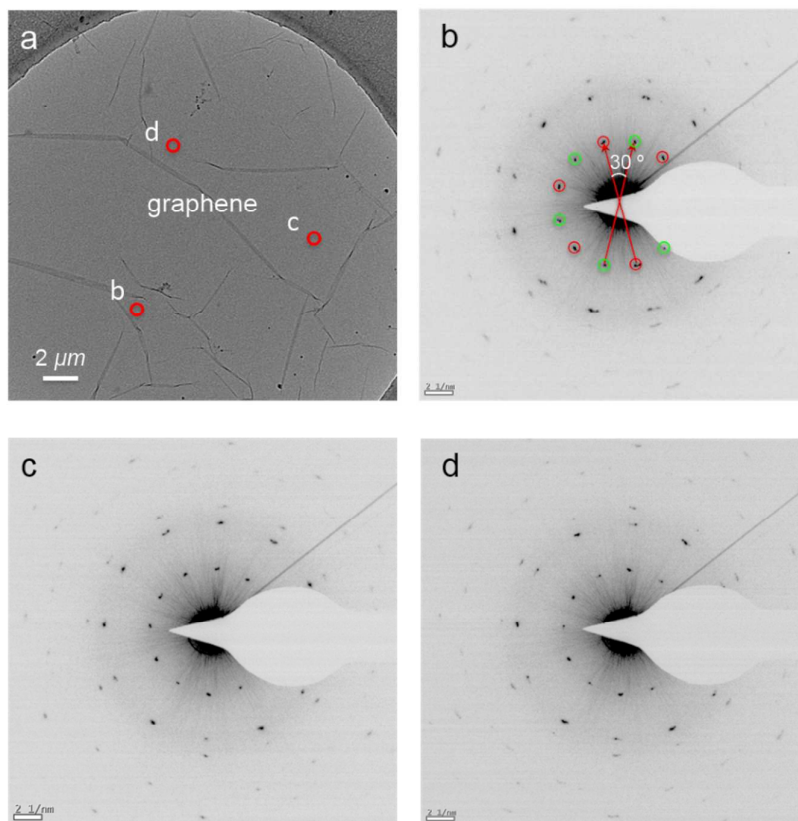
***Figure S4. Transmission electron microscope (TEM) evidence of the 30° relative rotational nature of most graphene domains. (a)** Low magnitude TEM image of the transferred graphene film. **(b-d)** Selected area electron diffraction (SAED) patterns of the graphene sample shown in (a).*

As we mentioned in the manuscript, most graphene domains (~70%) are rotated with each other by 30° according to STM observations. Herein, the TEM evidences are also presented in **Figure S4** for transferred samples on Cu grids, by using the same PMMA-assisted transfer method as reported before.[8] The large-area TEM image in **Figure S4a** shows that the transferred graphene film is nearly continuous and flat except for the appearance of some graphene wrinkles that may be generated from the transfer process. Corresponding SAED data of such regions (the diameter of the SEAD spot is ~ 200nm) (**Figure S4b-d**) convinces that there are two sets of diffraction patterns for graphene (marked as red and green circles, respectively), and they are 30° rotated with each other.

In this regard, we have reconfirmed the fact that, most of the graphene domains are indeed 30º rotated even after the sample transfer process, which is in good agreement with the STM observations based on the as-grown graphene/Au foil sample.
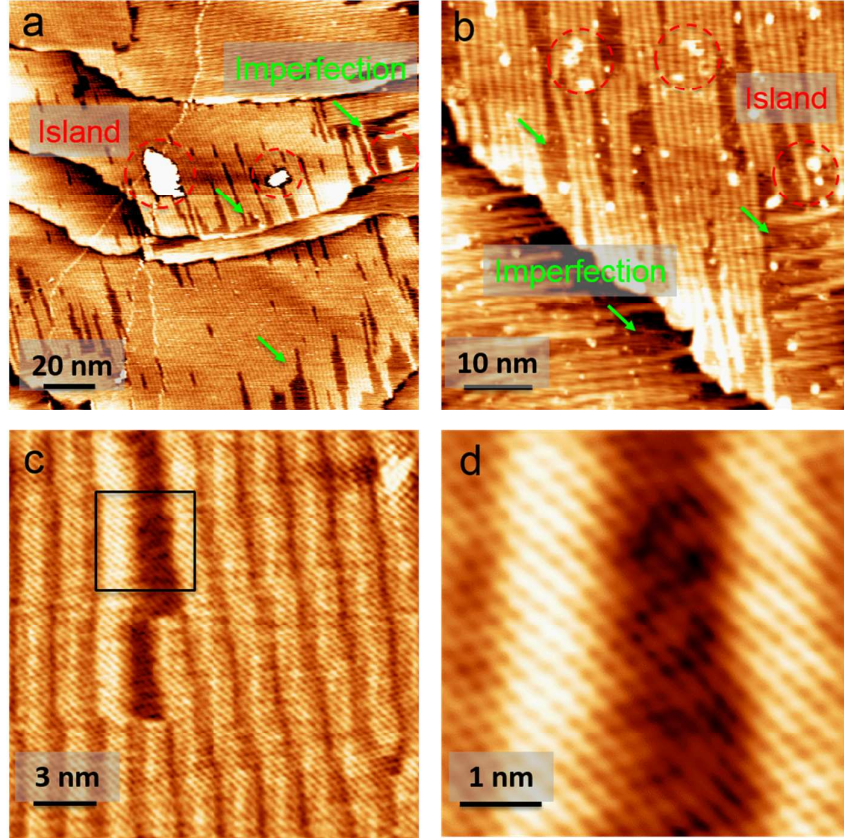

***Figure S5. Additional STM data of graphene covered on the imperfect hex-reconstructed Au (001) facet. (a, b)** Large-scale STM images of the surface (-0.83V, 1.88nA, 300K, 243 nm × 243 nm; 0.5V, 0.41 nA, 300K, 60 nm × 60 nm, respectively). **(c)** Atomic-resolution STM image of graphene covered on imperfect hex-reconstructed Au(001) facet (-0.06V, 4.87 nA, 300K, 18 nm × 18 nm). **(d)** Further zoom-in STM image of the rectangle part area in (c) showing continuous graphene lattice riding over the transitional region.*

As seen from the large-scale STM images (**Figure S5a, b**), the quasi-one-dimensional graphene superlattice are sometimes disturbed, with the occurrence of some "valley-like" areas near the step edges of Au(001), as indicated by the green arrows. This is probably mediated by the transition from hex-reconstructed Au(001)

to non-reconstructed Au(001), according to the published reference.[9] As known that, the atoms of hex-reconstructed Au(001) are more closely packed compared to that of the none-reconstructed Au(001) (~1.25 times). When this transition has taken place, some extra Au atoms (~25%) turn to form small islands on the surface, as indicated by the red circles in **Figure S5a, b**.[9]

Moreover, the experimental data also presents the fact that, in these imperfection areas (valley-like), graphene's characteristic honey-comb lattice still remains (black rectangle in **Figure S5c**). This indicates that graphene remains continuous and undestroyed even across these "valley-like" areas (**Figure S5d**).
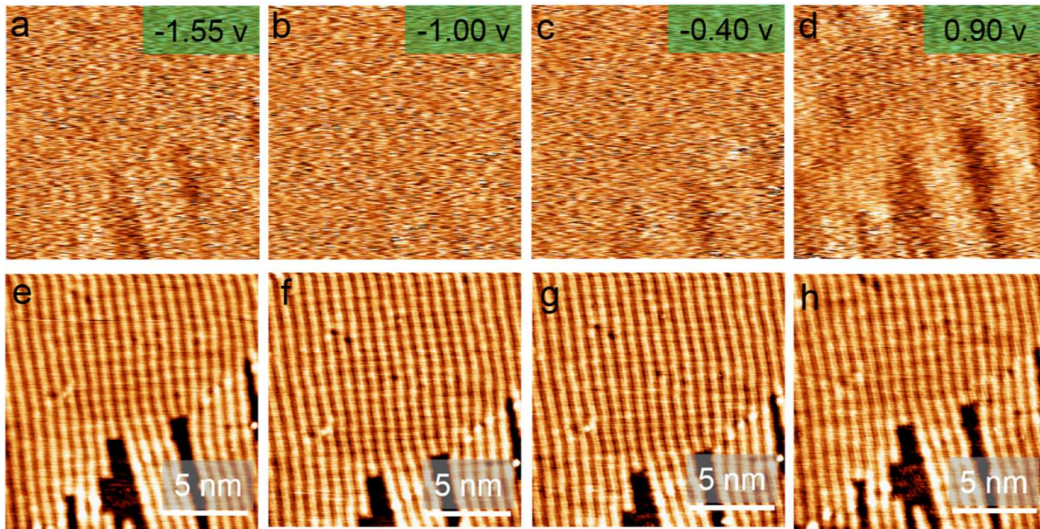

Figure S6. STS maps of graphene on a mixed hex-Au(001) and Au(001) surface. These maps are measured from the same surface of Figure 4a under different sample biases: -1.55 V for (a); -1.00 V for (b); -0.40 V for (c); 0.90 V for (d). (I_T = 0.70 nA; T = 78K, V_{rms} = 10 mV, f = 932 Hz; 35nm×35nm). (e), (f), (g), (h) are the original STM images for (a), (b), (c), (d), respectively.

As presented in **Figure S6**, the spatial variation of the new Dirac points for graphene riding over both hex-Au(001) and Au(001) regions is visible with the sample bias close to -1.7 and 1.1V, namely at -1.55 and 0.90V, respectively. In order to give a more precise description of this spatial variation, each dI/dV map is companied by its own STM image labeled with (e), (f), (g), (h), respectively. Basically, the new Dirac points should correspond to the vanishing of the density of

states (DOS) when the Fermi level was moved right at the locations (-1.73V and 1.12V).[10] This phenomenon could be noticed from **Figure 4b, c,** the dips of the dI/dV intensity (corresponding to the two new Dirac points) are usually accompanied by two neighboring peaks around them, herein at ~ -1.55V or ~0.9V, respectively. These two peaks show up and disappear synchronously with the new Dirac points, which could be used to understand the spatial variation of the two new Dirac points.

When the sample bias is set at ~ -1.55V, graphene on the reconstructed region presents a brighter contrast than that on the unreconstructed region (**Figure S6a**). This is because the graphene on hex-Au(001) are characterized with new Dirac points (at -1.73V), followed with enhanced dI/dV peak (at -1.55V). A similar contrast difference could be observed at the ~ 0.90V mapping image (**Figure S6d**). While, at other sample biases (1.00V and -0.40V), the contrast difference between the two typical regions are almost invisible.

In brief, the spatial variation of the new Dirac points is extremely sensitive to the hex-reconstruction of Au(001).
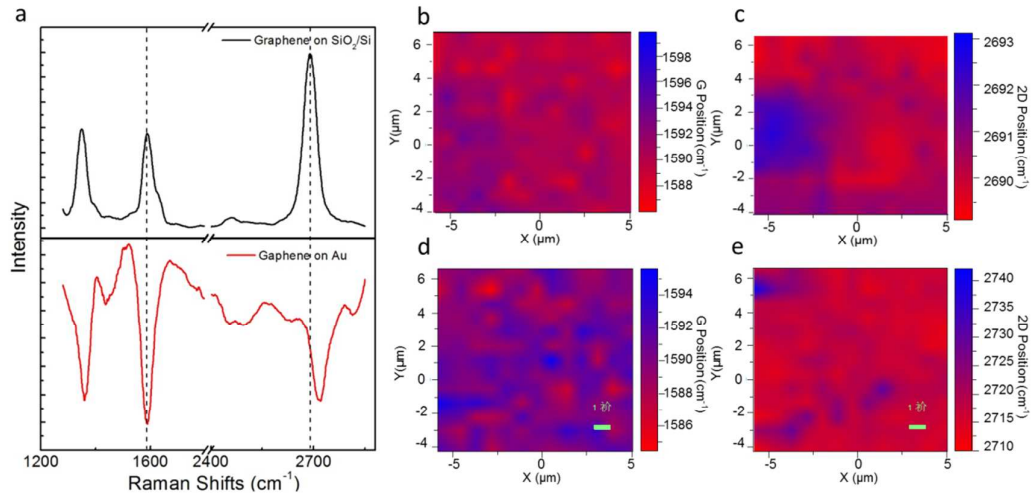
Figure S7 *Raman data for addressing the strain effect in graphene/Au foil system. **(a)** Typical Raman spectrum of graphene on Au foil (red) and after transferring onto SiO₂/Si (black). The Raman mapping images of G and 2D peak positions for transferred graphene on SiO₂/Si are presented in **(b)** and **(c),** respectively. The corresponding Raman mapping images of G and 2D peak positions of graphene on Au*

foil are presented in (d) and (e), respectively.

In order to clarify the existence of strain in graphene/Au foils, we have finished Raman measurements for graphene directly grown on Au foils and after transferred onto SiO_2/Si substrates. Many literatures have proved that the positions of G peak and 2D peak are very sensitive to the strain. As presented in **Figure S7a,** two facts are revealed, 1) the difference of the G peak positions between the two samples are very small, only ~2cm^{-1} blue shift of graphene on Au foil (1590cm^{-1}) compared to that on SiO_2/Si (1588cm^{-1}), 2) the difference of 2D peak position between the two samples are very obvious, nearly ~20 cm^{-1} blue shift of graphene on Au foils (2710cm^{-1}) compared to that on SiO_2/Si (2690cm^{-1}). This result is highly comparable to the work by X. F. Han *et al.*[11]

According to references,[12,13] if the shift of the G peak is more obvious than that of the 2D peak, this shift can be explained from the interface charge-transfer effect rather than mechanical strain. Namely, the shift of 2D peak would be more evident than that of the G peak when the strain effect dominates.[14-16] In our case, the ~20cm^{-1} blue shift of 2D peak is much stronger than the ~2cm^{-1} blue shift of G peak. This can be an evidence of the existence of compress strain in the graphene/Au system. Furthermore, the mapping images of **Figure S7b,c,d,e** present relative uniform color contrasts, indicating that the strain dispersion is relative uniform on the as-grown sample.

After convincing the existence of compress strain in graphene/Au, we are curious about the magnitude of the strain and its effect on the electronic structure of graphene. Fortunately, some works have already addressed this issue, according to Hilke *et al.*[17] the compress strain should be between -0.5% and -0.4% when the 2D peak is about 2710 cm^{-1} (in line with our graphene/Au system). Notably, this strain is too small to induce an obvious change of the electronic property, and at least over 20% strain is needed to induce a bandgap opening.[18,19] According to the theoretical calculation,[18] the Fermi velocity shows almost no anisotropic effect when the strain is smaller than 1%. The shape of the energy band should maintain the typical Dirac cone structure.

In a brief summary, the compress strain (estimated as -0.4%) should exist in our

graphene/Au system. However, such a small strain should have little influence on the electronic structure of graphene.

References

1. Shi, J.; Ma, D.; Han, G.-F.; Zhang, Y.; Ji, Q.; Gao, T.; Sun, J.; Song, X.; Li, C.; Zhang, Y., Controllable Growth and Transfer of Monolayer MoS_2 on Au Foils and Its Potential Application in Hydrogen Evolution Reaction. *ACS Nano* **2014**, *8*, 10196-10204.

2. Geng, H.-Z.; Kim, K. K.; So, K. P.; Lee, Y. S.; Chang, Y.; Lee, Y. H., Effect of Acid Treatment on Carbon Nanotube-Based Flexible Transparent Conducting Films. *J. Am. Chem. Soc.* **2007**, *129*, 7758-7759.

3. K, DETERT, Investigations on A New Kind of Secondary Recrystallization in Iron-3% Silicon Alloys. *Acta Metall*. **1959**, *7*, 589.

4. DALE, K., Promotion of Cubic Grain Growth in 3% Silicon Iron by Control of Annealing Atmosphere Composition. *J. Appl. Phys*. **1960**, *31*, 408.

5. Graham, C. D.; Chairman, Jr.; Walter, J. L, Metal and Alloy: Control of Texture in Magnetic Material by Surface Energy. *J. Appl. Phys*. **1965**, *36*, 1213.

6. C. S. Barrett, T.B. Massalski, *Structure of Metals: Crystallographic Methods, Principles and Data, Third Revised Edition*; Pergamon Press: New York, 1980; pp 578-579.

7. Hammer, R.; Sander, A.; Förster, S.; Kiel, M.; Meinel, K.; Widdra, W., Surface Reconstruction of Au (001): High-Resolution Real-Space and Reciprocal-Space Inspection. *Phys. Rev. B* **2014,** *90*, 035446.

8. Li, X.; Zhu, Y.; Cai, W.; Borysiak, M.; Han, B.; Chen, D.; Piner, R. D.; Colombo, L.; Ruoff, R. S., Transfer of Large-Area Graphene Films for High-Performance Transparent Conductive Electrodes. *Nano Lett.* **2009**, *9*, 4359-4363.

9. Jiang, Y.; Liang, X.; Ren, S.; Chen, C.-L.; Fan, L.-J.; Yang, Y.-W.; Tang, J.-M.; Luh, D.-A., The Growth of Sulfur Adlayers on Au (100). *J. Chem. Phys.* **2015**, *142*, 064708.

10. Park, C.-H.; Yang, L.; Son, Y.-W.; Cohen, M. L.; Louie, S. G., Anisotropic Behaviours of Massless Dirac Fermions in Graphene Under Periodic Potentials. *Nat.*

Phys. **2008**, *4*, 213-217.

11. Wang, W. X.; Liang, S. H.; Yu, T.; Li, D. H.; Li, Y. B.; Han, X. F., The Study of Interaction Between Graphene And Metals by Raman Spectroscopy. *J. Appl. Phys.* **2011**, *109*, 07c501.

12. Stampfer, C.; Moliter, F.; Graf, D.; Ensslin, K.; Jungen, A; Hierold, C.; Wirtz, L., Raman Imaging of Doping Domains in Graphene on SiO_2. *Appl. Phys. Lett.* **2007**, *91*, 241907.

13. A. Das; S. Pisana; B. Chakraborty; S. Piscanec; S. K. Saha; U. V. Waghmare; K. S. Novoselov; H. R. K.; A. K. Geim; A. C. Ferrari; A. K. Sood, Monitoring Dopants by Raman Scattering in An Electrochemically Top-Gated Graphene Transistor. *Nat. Nanotechnol.* **2008**, *3*, 210-215.

14. Huang M.; Yan H.; Chen C.; Song D.; Heinz T. F.; Hone J., Phonon Softening and Crystallographic Orientation of Strained Graphene Studied by Raman Spectroscopy. *Proc. Natl. Acad. Sci. U. S. A.* **2009**, *106*, 7304-7308.

15. Yu, T.; Ni, Z.; Du, C.; You, Y.; Wang, Y.; Shen. Z., Raman Mapping Investigation of Graphene on Transparent Flexible Substrate: The Strain Effect. *J. Phys. Chem. C.* **2007**, *112*, 12602-12605.

16. M, T. M. G.; Lombardo, A.; Nair, R. R.; Bonetti, A.; Savini, G.; Jalil, R.; Bonini, N.; Basko, D. M.; Galiotis, C.; Marzari, N.; Novoselov, K. S.; Geim, A. K.; Ferrari, A. C., Uniaxial Strain in Graphene by Raman Spectroscopy: G Peak Splitting, Grüneisen Parameters, and Sample Orientation. *Phys. Rev. B* **2009**, *79*, 205433.

17. V. Yu; E. Whiteway; J. Maassen; M. Hilke, Raman Spectroscopy of the Internal Strain of A Graphene Layer Grown on Copper Tuned by Chemical Vapor Deposition. *Phys. Rev. B* **2011**, *84*, 205407.

18. Seon-Myeong Choi; Seung-Hoon Jhi; Young-Woo Son, Effects of Strain on Electronic Properties of Graphene. *Phys. Rev. B* **2010**, *81*, 081407(R).

19. Vitor M. Pereira;A. H. Castro Neto, Tight-Binding Approach to Uniaxial Strain in Graphene. *Phys. Rev. B* **2009**, *80*, 045401.